Food Research International xxx (xxxx) xxx–xxx

Contents lists available at ScienceDirect

Food Research International

journal homepage: www.elsevier.com/locate/foodres

Effects of lipids on the water sorption, glass transition and structural strength of carbohydrate-protein systems

V.A. Maidannyk[a,b], A.S.L. Lim[a,b], M.A.E. Auty[a], Y.H. Roos[b,*]

[a] Food Chemistry & Technology Department, Teagasc Food Research Centre, Moorepark, Fermoy, Co. Cork, Ireland.
[b] School of Food and Nutritional Sciences, University College Cork, Cork, Ireland.

ARTICLE INFO

Keywords:
WLF
CLSM
SEM
Relaxations
Encapsulant system
Glass former strength

ABSTRACT

Encapsulant systems are gaining wide practical interest due to their functional and nutritional properties. This paper was focusing on understanding structural relaxations in that systems near glass transition temperature. Freeze-dried trehalose-whey protein isolate-sunflower oil systems with various ratios of the last were used as a carbohydrate-protein-lipid food model. The Guggenheim-Anderson-de Boer (GAB) water sorption relationship was used as a tool to model water sorption isotherms. The glass transition temperature was obtained by differential scanning calorimetry (DSC). Structural α-relaxation temperatures were measured by dynamical mechanical analyses (DMA), dielectric analysis (DEA) and combined to cover a broad range for strength assessment. The microstructure was characterized by optical light microscopy, confocal laser scanning microscopy and scanning electron microscopy. The C_1 and C_2 constants for Williams-Landel-Ferry (WLF) equation and structural strength parameter were calculated for each system. The effect of sunflower oil and water contents on strength of carbohydrate-protein system was analyzed. Strength shows decreasing with increasing of lipid concentration in the mixtures and more complex dependence on the water content in a system.

1. Introduction

Carbohydrates, proteins and lipids are the common macronutrients present in most food solids, including dairy powders and infant formulas. There are a number of key processes such as freeze-drying, spray drying and extrusion which can be used for encapsulation of lipid components (Roos, 2010). Glass transition temperature (T_g) is an important parameter which characterizes the range of temperatures over which amorphous solids (e.g. glass) are converted to supercooled liquids (e.g. rubber) showing viscous flow with rapid changes in structural relaxation times at increasing temperature (Angell, Ngai, McKenna, McMillan, & Martin, 2000; Roos, 2008). Despite the fact that T_g is an important characteristic it does not provide kinetic information about structural relaxation processes. Hence, studying relaxation times of mechanical, electrical and thermal properties is required for a deeper understanding of the materials. Roos et al. (2015) proposed a simple mathematical approach, which combine temperature and practically important time factors. This structural "strength" (S) concept was introduced to describe the critical temperature difference to the T_g where structural relaxation times become equal to critical real-time macroscopic transformations (Fan & Roos, 2016, 2017; Maidannyk, Nurhadi, & Roos, 2017; Maidannyk & Roos, 2016, 2017, 2018; Roos et al., 2015). Such information is suitable for understanding food materials properties and performance affecting food stability and flow behavior in industrial applications.

In the present study trehalose-whey protein isolate (WPI) system with various levels of sunflower oil (SO) were used to investigate structural relaxations near the T_g. Trehalose is a naturally occurring disaccharide with a high glass transition temperature. It has unique properties such us stabilizing protein structures and membrane structures in a dry state, resulted in inhibition biological damage (Crowe, Crowe, Rudolph, Womersley, & Appel, 1985; Green & Angell, 1989; Xie & Timasheff, 1997). Bovine whey proteins have very complex protein structures and consist of β-lactoglobulin ~ 50%, α-lactalbumin ~ 20%, bovine serum albumin ~ 10% as well as smaller quantities of lactoferrin and other proteins. A mix of whey proteins does not have clear representative T_g (Maidannyk & Roos, 2016; Roos & Potes, 2015). Carbohydrate solids and proteins, as glass-forming food components, are often used to obtain hydrophilic encapsulant solid matrices, which have important function as continuous phase during encapsulation (Vega & Roos, 2006). These amorphous substances have the ability to encapsulate or entrap volatile, bioactive and flavor compounds. SO as a liquid lipid can be dispersed into carbohydrate-protein continuous phase where it may affect protein assembly within the system

* Corresponding author.
E-mail address: yrjo.roos@ucc.ie (Y.H. Roos).

https://doi.org/10.1016/j.foodres.2018.10.008
Received 30 April 2018; Received in revised form 25 September 2018; Accepted 2 October 2018

(Cornacchia & Roos, 2011).

Water, as a universal solvent, is an excellent plasticizer for many amorphous food systems and have a very low commonly agreed T_g (−135 °C) (Debenedetti, 2003). Since, T_g of complex multicomponent systems depends on miscibility of components, the presence of water significantly decreases T_g of hydrophilic food components (Roos, 2008). Proteins are macromolecules which interact differently with water from small carbohydrates molecules (Swenson & Cerveny, 2015). Due to hydrophobic structures, proteins have poor miscibility and molecular segregation with aqueous carbohydrates (Halle, 2004; Roos & Potes, 2015). On the other hand, the presence of lipids in dispersed phase of carbohydrate-protein system slightly decreases T_g (Potes, Kerry, & Roos, 2014).

Differential scanning calorimetry (DSC) is a common method in T_g determination. Unfortunately, for high water content systems (> 50 g/100 g of dry solids) the determination of T_g is practically very difficult. For these aqueous systems, the Gordon-Taylor equation can predict T_g values (Arvanitoyannis, Blanshard, Izzard, Lillford, & Ablett, 1993). At temperatures below T_g, the amorphous structures are fairly stable in the glassy state (Roos & Drusch, 2015; Slade, Levine, & Reid, 1991; Sperling, 2005). However, structural changes such as stickiness, collapse, crystallization and caking happen in amorphous materials at temperatures above T_g (Fan & Roos, 2017; Özkan, Walisinghe, & Chen, 2002; Prado, Buera, & Elizalde, 2006). Changes in mechanical and electric properties during these processes around T_g result in α-relaxation which can be detected by dynamic mechanical (DMA) and dielectric (DEA) analyses in a multi-frequency mode. These methods are suitable for many carbohydrates with different water contents (Ermolina, Polygalov, Bland, & Smith, 2007; Kilmartin, Reid, & Samson, 2004; Potes, Kerry, & Roos, 2012; Silalai & Roos, 2011). For amorphous powders, the structural relaxation time can be calculated from frequency of primary α-relaxation (Noel, Parker, & Ring, 2000).

Optical light microscopy (OLM) with polarized light is a common technique which allows distinguishing crystalline structure from amorphous material (Hartel, 2001; Maher, Auty, Roos, Zychowski, & Fenelon, 2015). Confocal laser scanning microscopy (CLMS) and scanning electron microscopy (SEM) are useful methods to study microstructural differences in various food products (cheeses, milk powders, infant formulae, coffees, chocolates etc.) due to significant differences in food structure surface such as the distribution of fat globules (Auty, Twomey, Guinee, & Mulvihill, 2001; Maher et al., 2015; Soottitantawat, Yoshii, Furuta, Ohkawara, & Linko, 2003).

Our previous studies showed that structural strength approach can be successfully applied for various food systems including carbohydrate-protein (trehalose-WPI; lactose-WPI), miscible carbohydrate (lactose-trehalose; trehalose-maltodextrin) and partially crystalline (trehalose) systems (Fan & Roos, 2016, 2017; Maidannyk et al., 2017; Maidannyk & Roos, 2016, 2017, 2018). These studies have confirmed that composition and water contents significantly influence structural strength parameter (S). However, the effect of lipids on structural strength has not been addressed. Hence, the main purpose of the present study was to apply structural strength analysis, including water sorption, glass transition, dielectric, mechanical measurements and observations of microstructure to amorphous carbohydrate-protein-lipid systems. The effect of water on the S parameter for systems with varied amount of SO was also addressed.

2. Materials and methods

2.1. Materials

D-(+)-Trehalose crystalline dihydrate (Hayashibara Co., Ltd., Okayama, Japan), whey protein isolate (Isolac®, Carbery Food Ingredients, Ballineen, Cork, Ireland) and sunflower oil (Musgrave Excellence™, Spain) were used without purification. De-ionized water was obtained from KB scientific, Cork, Ireland.

Table 1
The composition (% of mass, in total) of components during emulsion preparation and final composition of emulsion.

	System 1	System 2	System 3
Pre-emulsion			
WPI	2.4	2.4	2.4
Sunflower oil	0	10	20
Water	42.6	32.6	22.6
Wall material			
Trehalose	6	6	6
WPI	4	4	4
Water	45	45	45
Final emulsion composition			
Trehalose	6	6	6
WPI	6.4	6.4	6.4
Sunflower oil	0	10	20
Water	87.6	77.6	67.6

Table 2
Water content of freeze-dried trehalose-WPI-SO emulsions (systems 1, 2, 3) stored at different water activities (0.11, 0.23, 0.33, 0.44, 0.55, 0.65, 0.76, 0.85) for 360 h at 25 ± 2 °C.

Experimental water content (g/100 g of solids not fat)			
a_w	System 1	System 2	System 3
0.11	3.37 ± 0.27	3.15 ± 0.59	3.01 ± 0.32
0.23	5.47 ± 0.37	5.35 ± 0.25	5.18 ± 0.21
0.33	7.59 ± 0.44	7.35 ± 0.21	6.96 ± 0.26
0.44	10.01 ± 0.27	9.14 ± 0.31	9.02 ± 0.27
0.545	12.27 ± 0.33	11.56 ± 0.38	11.45 ± 0.38
0.65	14.71 ± 0.41	14.56 ± 0.37	11.99 ± 1.42
0.76	15.21 ± 0.28	15.18 ± 0.51	15.17 ± 0.27
0.86	21.84 ± 0.35	20.23 ± 0.84	17.73 ± 0.53

2.2. Determination of the initial water content

Powders of trehalose and WPI (0:100; 50:50 and 100:0 trehalose-WPI systems) with final mass 0.5–1.0 g were dried at 70 °C with absolute pressure P_{abs} < 10 mbar for 24 h in a WTB Binder vacuum oven (Mason Technology®, Tuttingen, Germany) to measure the initial water content of the materials. The difference in mass of samples before and after drying (g/100 g of dry solids) was defined as initial water content.

2.3. Emulsion preparation

The main principle of emulsion preparation was the addition of different amounts of SO to the systems with the same trehalose:WPI (50:50) ratio (Table 1). There were three main stages of the emulsion preparation: (I) Production of pre-emulsion; (II) Preparation of wall materials and (III) Final emulsion preparation. Emulsion preparation was done as detailed by Lim, Burdikova, Sheehan, and Roos (2016) with slight adjustments.

2.3.1. Production of pre-emulsion

Deionized water was used to disperse WPI (5.6, 7.4 and 10.6% *w/w* for system 1, 2 and 3 respectively) and the dispersion was left to hydrate for 2 h. SO *(0; 10 and 20% w/w of total emulsion mass for system 1, 2 and 3 respectively)* was used as a lipid phase. The water and oil phases at the ratio 33:40 were then mixed for 60 s with IKA® T25 digital ultra-turrax® mixer (Germany) at 10^3 rpm to produce pre-emulsions. Homogenization of pre-emulsion was done at 240 bars (200 bars for the first stage and 40 bars for the second) at room temperature using a two-stage valve homogenizer (APV-1000, APV Homogenizer Group, Wilmington, MA, USA).

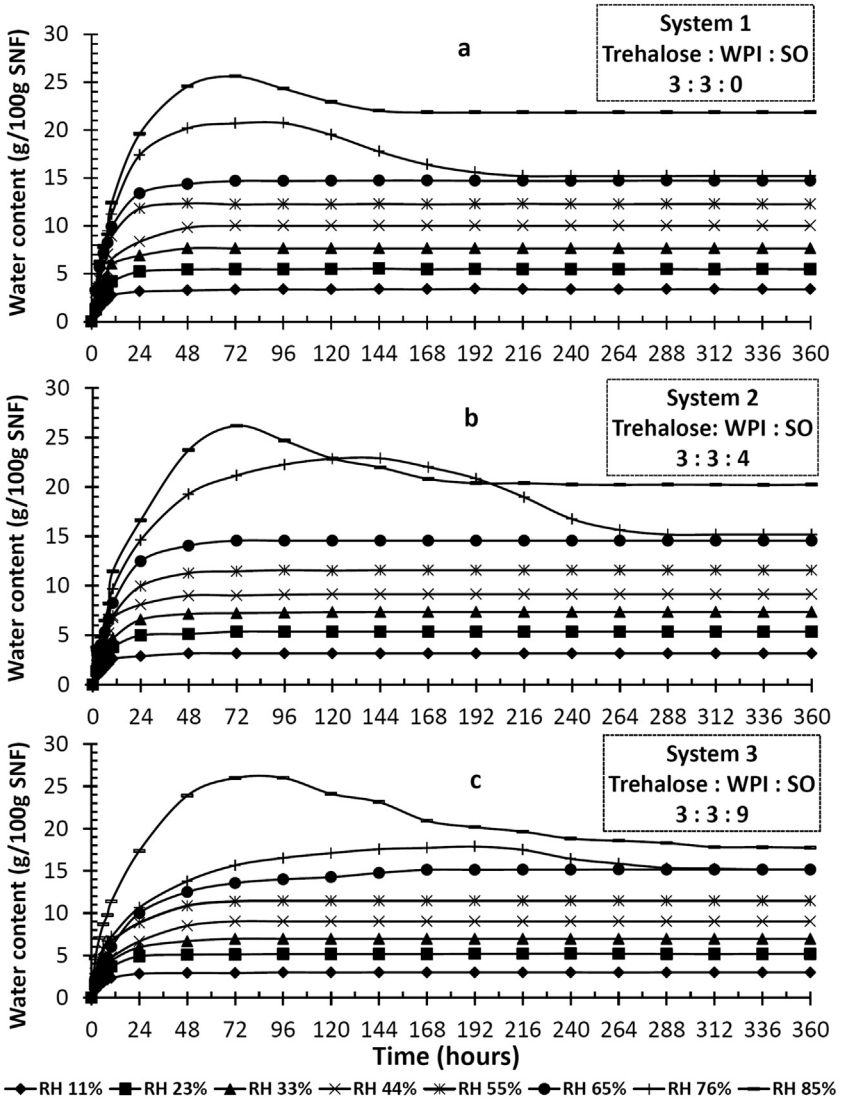

Fig. 1. Sorption kinetics profiles for freeze-dried trehalose-WPI-SO system 1(a), 2(b) and 3 (c) stored at 0.11, 0.23, 0.33, 0.44, 0.55, 0.65, 0.76 and 0.85 a_w, monitored during 360 h at 25 ± 2 °C.

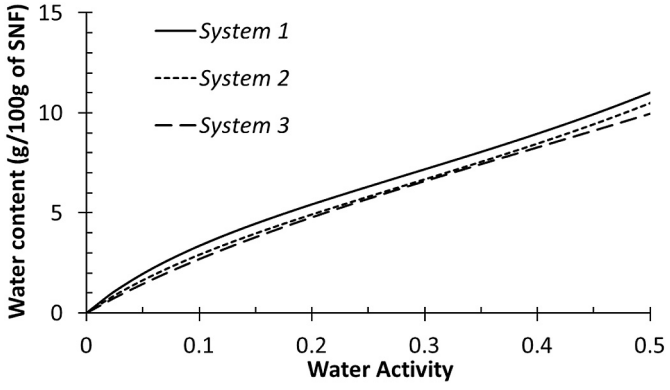

Fig. 2. Water sorption isotherms (25 ± 2 °C) for freeze-dried trehalose-WPI-SO system 1, 2 and 3. The isotherms were modeled using the GAB equation with experimental data.

2.3.2. Preparation of wall material

Trehalose (56.6% w/w of total solids, in water) and WPI (11.4% w/w in water) were used as wall materials. Trehalose was dissolved and WPI was dispersed (2 h) in deionized water, followed by mixing (with magnetic stirrer) for 30 min.

Table 3
Measured by DSC the onset of calorimetric glass transition temperatures (T_g) of freeze-dried (0 a_w) and humidified (0.11–0.44 a_w) trehalose-WPI-SO systems stored for 360 h at 25 ± 2 °C.

Glass transition temperatures (T_g), °C			
a_w	System 1	System 2	System 3
0	119 ± 3	123 ± 7	126 ± 6
0.11	48 ± 6	51 ± 8	54 ± 3
0.23	35 ± 4	37 ± 6	38 ± 5
0.33	25 ± 3	28 ± 4	30 ± 5
0.44	18 ± 4	19 ± 5	21 ± 6

2.3.3. Final emulsion preparation

The wall material mixture was added into homogenized pre-emulsion at the ratio 55:45 or 11:9 and mixed for 30 min with magnetic stirrer to obtain the final emulsions.

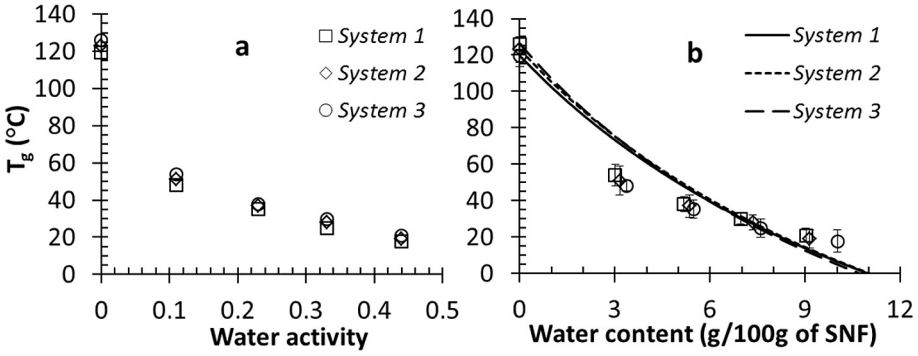

Fig. 3. Effects of water activity (a) and water content (g/100 g of SNF) (b) on the onset T_g in anhydrous and humidified trehalose-WPI-SO systems 1, 2, 3 stored for 360 h at 25 ± 2 °C. Lines correspond to the T_g predicted by Gordon-Taylor equation.

2.4. Preparation of amorphous freeze-dried materials

5 ml aliquots of each emulsion (system 1, 2, 3) were frozen in pre-weighted and semi-closed with septum 10 ml glass vials at −20 °C for 24 h, then at −80 °C for 4 h, followed by freeze-drying for 60 h at pressure $p < .1$ mbar (Lyovac GT2, Steris®, Hürth, Germany) to obtain amorphous materials (Maidannyk et al., 2017). All vials were hermetically sealed under the vacuum conditions inside the freeze-dryer at $p < .1$ mbar and stored over P_2O_5 in vacuum desiccators (Roos & Karel, 1990) at room temperature (25 ± 1 °C) to protect samples from water uptake.

2.5. Water sorption analysis

Hermetically sealed freeze-dried and closed under vacuum samples of different emulsion systems were stored in desiccators over P_2O_5. Each system was stored in an evacuated desiccator (25 ± 1 °C) for 10 days over the saturated solutions of LiCl, CH_3COOK, $MgCl_2$, K_2CO_3, Mg $(NO_3)_2$, $NaNO_2$, NaCl and KCl (Sigma Chemical Co., St. Louise, MO. U.S.A.), which at equilibrium provided 0.11, 0.23, 0.33, 0.44, 0.545, 0.66, 0.76 and 0.85 a_w respectively. AQUALAB 4 (TE) (Decagon Devices Inc., NE) water activity meter was used to measure water activity for each material after storage. Samples were weighted at intervals of 0, 2, 4, 6, 8, 10, 24, 48, 72 and then every 24 h for up to 360 h upon storage. Possible crystallization of trehalose was assessed from water sorption kinetics (Maidannyk et al., 2017). The water content in each mixture was plotted as a function of time, and the Guggenheim-Anderson-de Boer (GAB) relationship was fitted to data to relate water activity and water content of amorphous trehalose-WPI-SO systems (Eq. (1)):

$$\frac{m}{m_0} = \frac{Cka_w}{(1 - ka_w)(1 - ka_w + Cka_w)} \quad (1)$$

2.6. Differential scanning calorimetry (DSC)

Differential scanning calorimeter (DSC) (Mettler Toledo Schwerzenbach, Switzerland) was used to measure the glass transition temperature of amorphous trehalose-WPI-SO systems with 0, 0.11, 0.23, 0.33 and 0.44 a_w. Samples of all systems were transferred to pre-weighted standard DSC aluminium pans (40 μL, Mettler Toledo Schwerzenbach, Switzerland) and hermetically sealed. An empty punctured pan was used as a reference. For anhydrous systems, the lids of DSC aluminium pans were punctured to allow evaporation of residual water upon the measurement. All samples were scanned from ~ 30 °C below to over T_g region with 5 °C/min heating rate and cooled at 10 °C/min to initial temperature. Then, second heating scan was run to well above (> 50 °C) the T_g at 5 °C/min heating rate. The onset of T_g was determined by the STAR^e software version 8.10 (Mettler Toledo Schwerzenbach, Switzerland) (Maidannyk et al., 2017). The Gordon-Taylor equation was fitted to T_g data to model T_g for the initial emulsions.

$$T_g = \frac{w_1 T_{g1} + kw_2 T_{g2}}{w_1 + kw_2} \quad (2)$$

2.7. Dynamical mechanical analyses (DMA)

Dynamic mechanical analyzer (DMA) (Tritec 2000 DMA, Triton Technology Ltd., UK) was used to measure mechanical properties (E″ – loss modulus, E′ – storage modulus and tan δ = E″/E′) of anhydrous and humidified trehalose-WPI-SO systems (described above for the DSC experiments). The DMA instrument was balanced or set at zero to determine the zero displacement position before starting. Approximately 60 g of grinded samples were spread on a metal pocket-forming sheet (Triton Technology Ltd., UK). This sandwich sheet was fixed between the stationary and drive shaft clamps inside the measuring head of the DMA. Length, width and thickness were measured for each sample. All results were obtained using 1.43.00 DMA software version. To control the temperature, DMA was connected to a liquid nitrogen tank (1 l; Cryogun, Brymill Cryogenic Systems, Labquip Ltd., Dublin, Ireland). Samples were scanned from ~ 50 °C below to over the α-relaxation region with cooling rate of 5 °C/min and heating rate of 2 °C/min using the single cantilever bending mode (Fan & Roos, 2016, 2017; Maidannyk & Roos, 2016, 2017, 2018; Potes et al., 2012). The α-relaxation temperatures (T_α) were determined from peak of tan δ above the glass transition.

2.8. Dielectric analysis (DEA)

Samples (described above for DSC and DMA experiments) of each system were analyzed by dielectric spectrometer, DEA (DS6000, Triton Technology Ltd., UK) with titanium sample holders as the electrodes. The LCR meter (LCR-819) and the DEA instrument were calibrated at frequency 0.103 kHz with open-short circuit of the electrodes and zeroed in bridge RQ on a regular basis at 1 kHz with open-short circuit of the electrodes to ensure that the electrodes were ready for use (resistance value < 2 Ω). Approximately 100 mg of grinded samples were transferred onto the lower cup electrode (40 mm diameter) and then pressed with the upper electrode (33 mm diameter). Two electrodes were placed into a dielectric cell. The thickness (< 2 mm) was measured for each sample. The DEA was connected to a liquid nitrogen tank (1 l; Cryogun, Brymill Cryogenic Systems, Labquip Ltd., Dublin, Ireland). Samples were scanned from ~50 °C below to over the α-relaxation region with cooling rate of 5 °C/min and heating rate of 2 °C/min at frequencies of 0.1, 0.5, 1, 5, 10 and 20 kHz (Maidannyk et al., 2017; Potes et al., 2012; Silalai & Roos, 2011). The T_α was determined from the peak temperature above T_g of dielectric loss (ε″). All results were obtained by Triton Laboratory DEA software, version 1.0.330.

Table 4
α-Relaxation temperature (T_α) detected by DMA (0.1–10 Hz) and DEA (100.0–20,000.0 Hz) for systems 1, 2, 3 equilibrated at different relative humidities (RH).

		System 1	System 2	System 3
f, Hz	logτ, s	T_α, °C	T_α, °C	T_α, °C
RH 0%				
0.1	0.20	151 ± 5	151 ± 2	145 ± 3
0.5	−0.49	152 ± 2	151 ± 5	149 ± 2
1.0	−0.80	153 ± 2	152 ± 2	150 ± 3
2.0	−1.10	157 ± 5	155 ± 2	151 ± 2
5.0	−1.50	159 ± 2	156 ± 3	152 ± 2
10.0	−1.80	161 ± 2	157 ± 2	153 ± 3
100.0	−2.80	163 ± 4	158 ± 3	162 ± 3
500.0	−3.50	165 ± 2	162 ± 2	162 ± 4
1000.0	−3.80	166 ± 5	164 ± 3	163 ± 4
5000.0	−4.50	167 ± 3	165 ± 4	164 ± 3
10,000.0	−4.80	168 ± 2	165 ± 4	165 ± 3
20,000.0	−5.10	-	166 ± 5	166 ± 4
RH 11%				
0.1	0.20	74 ± 3	73 ± 5	77 ± 2
0.5	−0.49	75 ± 4	74 ± 3	77 ± 5
1.0	−0.80	76 ± 2	74 ± 2	78 ± 3
2.0	−1.10	77 ± 4	76 ± 2	78 ± 3
5.0	−1.50	79 ± 5	79 ± 3	79 ± 2
10.0	−1.80	80 ± 2	80 ± 5	79 ± 3
100.0	−2.80	82 ± 3	80 ± 3	80 ± 3
500.0	−3.50	84 ± 4	81 ± 3	81 ± 5
1000.0	−3.80	84 ± 5	83 ± 4	83 ± 4
5000.0	−4.50	87 ± 4	84 ± 5	84 ± 5
10,000.0	−4.80	88 ± 4	87 ± 5	87 ± 4
20,000.0	−5.10	90 ± 4	89 ± 4	89 ± 5
RH 23%				
0.1	0.20	52 ± 3	52 ± 1	52 ± 3
0.5	−0.49	53 ± 5	53 ± 2	52 ± 2
1.0	−0.80	56 ± 3	53 ± 3	54 ± 2
2.0	−1.10	58 ± 2	56 ± 2	55 ± 3
5.0	−1.50	60 ± 3	59 ± 3	58 ± 2
10.0	−1.80	62 ± 2	60 ± 2	60 ± 3
100.0	−2.80	65 ± 3	61 ± 4	61 ± 4
500.0	−3.50	65 ± 4	62 ± 5	61 ± 4
1000.0	−3.80	67 ± 5	62 ± 4	63 ± 5
5000.0	−4.50	69 ± 4	64 ± 4	64 ± 5
10,000.0	−4.80	72 ± 5	68 ± 4	68 ± 4
20,000.0	−5.10	73 ± 5	71 ± 5	70 ± 5
RH 33%				
0.1	0.20	41 ± 2	43 ± 2	44 ± 3
0.5	−0.49	43 ± 2	44 ± 3	45 ± 2
1.0	−0.80	45 ± 1	45 ± 2	46 ± 3
2.0	−1.10	46 ± 2	45 ± 2	47 ± 3
5.0	−1.50	49 ± 3	47 ± 3	48 ± 1
10.0	−1.80	51 ± 2	48 ± 2	48 ± 3
100.0	−2.80	51 ± 4	48 ± 5	48 ± 5
500.0	−3.50	53 ± 5	52 ± 4	49 ± 5
1000.0	−3.80	54 ± 5	53 ± 5	49 ± 4
5000.0	−4.50	55 ± 5	54 ± 5	48 ± 4
10,000.0	−4.80	57 ± 4	54 ± 4	48 ± 4
20,000.0	−5.10	59 ± 4	55 ± 5	49 ± 4
RH 44%				
f, Hz	logτ, s	T_α, °C	T_α, °C	T_α, °C
0.1	0.20	34 ± 2	34 ± 2	36 ± 3
0.5	−0.49	36 ± 2	35 ± 3	37 ± 3
1.0	−0.80	37 ± 2	35 ± 3	37 ± 2
2.0	−1.10	38 ± 3	36 ± 3	38 ± 3
5.0	−1.50	39 ± 3	38 ± 2	38 ± 3
10.0	−1.80	40 ± 2	39 ± 3	39 ± 3
100.0	−2.80	40 ± 5	37 ± 5	39 ± 3
500.0	−3.50	41 ± 4	37 ± 5	39 ± 5
1000.0	−3.80	41 ± 5	38 ± 4	39 ± 4
5000.0	−4.50	42 ± 5	39 ± 6	40 ± 5
10,000.0	−4.80	43 ± 4	40 ± 4	40 ± 6
20,000.0	−5.10	44 ± 5	40 ± 4	40 ± 4

To calculate the relaxation times (τ) of peak T_α, measured by DMA and DEA at various frequencies (f), we used the Eq. (3) (Maidannyk et al., 2017; Noel et al., 2000; Potes et al., 2012):

$$\tau = \frac{1}{2\pi f} \tag{3}$$

2.9. Microstructure

2.9.1. Optical light microscopy

Microscopy observation was done on anhydrous systems 1, 2, and 3 using an Olympus BX51 (Olympus Corporation, Tokyo, Japan) light microscope with 20× dry objective lens with polarized light. Digital images (TIFF, 8-bit) were taken and captured using Jenoptik C14 Imagic camera.

2.9.2. Confocal laser scanning microscopy

Leica TCS SP5 confocal laser scanning microscope (CLSM; Leica Microsystems CMS GmbH, Wetzlar, Germany) was used for powder particles visualization. Powder particles were placed onto a glass slide and labeled using a mixture of Fast Green and Nile Red (Auty et al., 2001; Maher et al., 2015). The dye mixture containing Fast Green (aq. 0.01 g/0.1 l) and Nile Red were dissolved in polyethylene glycol 400 g/mol (0.1 g/0.1 l)mixed in a ratio 1:40 of Fast Green to Nile Red, which allowed diffusion of the dye molecules into the particles whilst not influencing the particle morphology and preventing solubilization (Maher et al., 2015). Dual excitation at 488 nm/633 nm was used. The confocal images of each systems were taken using 63× oil immersion objective with numerical aperture 1.4 z-Stacks were obtained in order to generate a three-dimensional structure of the particle and to identify surface lipid staining (Maher et al., 2015). Red and Green pseudo-colored pictures (8-bit), 512 × 512 pixels in size, were acquired using a zoom factor of 1–3.

2.9.3. Scanning electron microscopy

Each freeze-dried trehalose-WPI-SO systems were attached to double-sided adhesive carbon tabs mounted on scanning electron microscope stubs, and then coated with chromium (K550X, Emitech, Ashford, UK). Scanning electron microscopy images were collected using a Zeiss Supra 40P field emission SEM (Carl Zeiss SMT Ltd., Cambridge, UK) at 2.00 kV. Representative micrographs were taken at 200×, 500×, 1000×, 5000× and 10,000× magnification.

2.10. Calculation of WLF model constants and Structural strength parameter

To calculate the structural strength parameter (S), the constants C_1 and C_2 from Williams Landel Ferry (WLF) equation were obtaining as described by Roos and Drusch (2015).

The WLF equation in the form of (Eq. (5)) was used to fit DMA and DEA data (Williams, Landel, & Ferry, 1955):

$$log_{10}\frac{\tau}{\tau_s} = log_{10}\frac{\eta}{\eta_s} = \frac{-C_1(T - T_g)}{C_2 + (T - T_g)} \tag{5}$$

where, τ is relaxation time, τ_s is reference relaxation time, η is viscosity, η_s is reference viscosity, T is temperature, T_g is glass transition temperature, C_1 and C_2 are constants.

The WLF equation in the form of (Eq. (6)) suggested that the plot of $1/\lg(\tau/\tau_s)$ versus $1/(T\text{-}T_g)$ gives a linear correlation:

$$\frac{1}{lg\frac{\tau}{\tau_s}} = \frac{1}{-C_1} - \frac{C_2}{C_1(T - T_g)} \tag{6}$$

The WLF constants C_1 and C_2 were derived from the slope and intercept (Roos & Drusch, 2015).

Mathematically, S is based on WLF relationship and can be

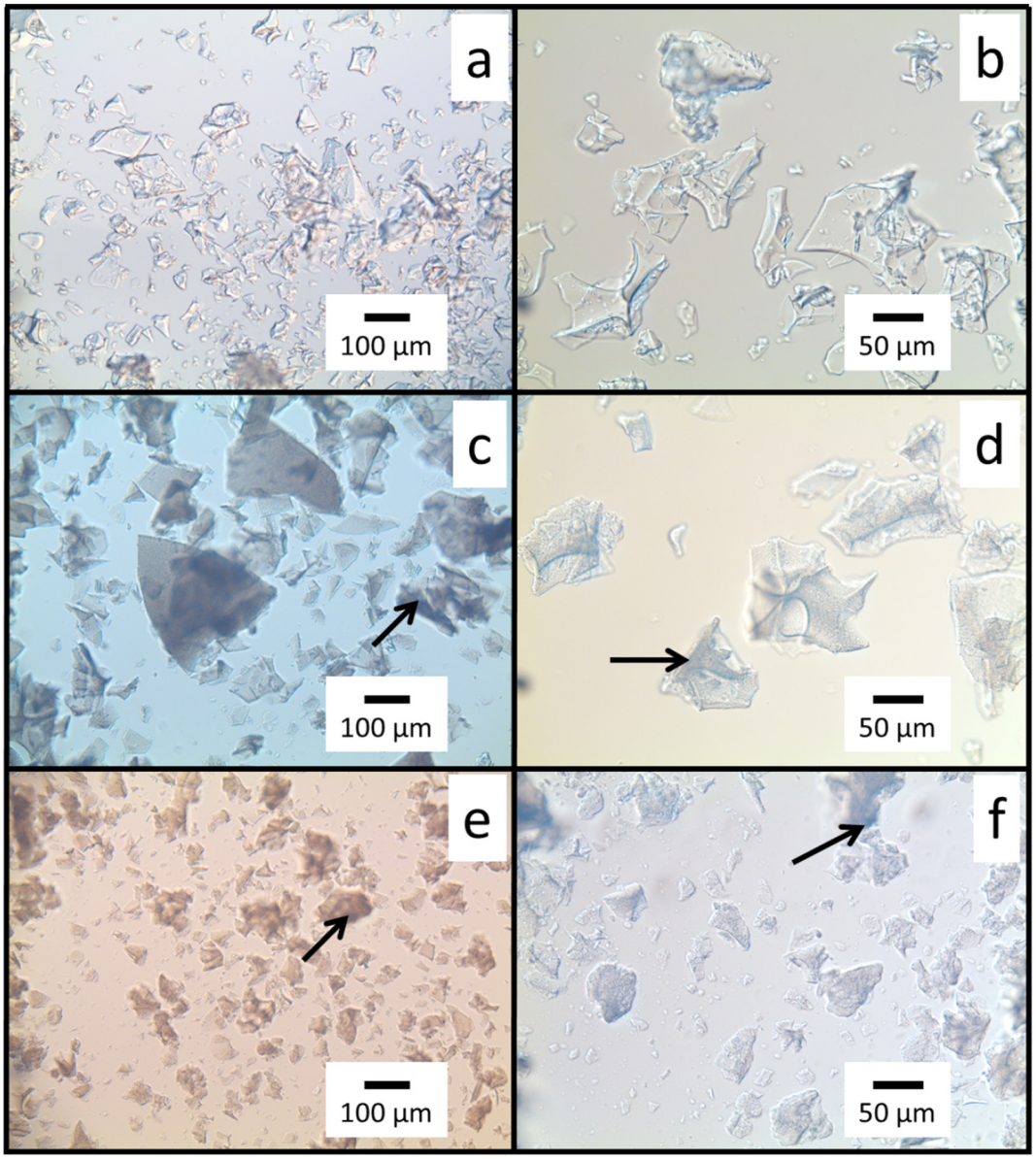

Fig. 4. Optical light micrographs of anhydrous freeze-dried trehalose-WPI-SO systems 1 (a, b), 2 (c, d) and 3 (e, f). Arrows indicate SO drops.

calculated by Eq. (6):

$$S = \frac{dC_2}{C_1 - d} \tag{7}$$

where d is a parameter, showing the critical decrease in the number of logarithmic decades for the flow (e.g., 100 s to 0.01 s corresponds to $d = 4$; can be chosen for each system as an integer depending on the critical time for the process (Fig. 7)), C_1 and C_2 are "non-universal" constants in the WLF equation.

Eq. (8) was used to predict structural strength at different water contents:

$$S = \frac{w_1 S_1 + k w_2 S_2}{w_1 + k w_2} \tag{8}$$

where w_1 – weight fraction of dry solid; w_2 – weight fraction of water; k – coefficient; S_1 – structural strength for anhydrous system; S_2 – structural strength of pure water ($S_2 = 6.0$) (Maidannyk et al., 2017).

2.11. Data analysis

All experiments were performed in triplicate. Mean data of the water sorption analyses, DSC, DMA and DEA were calculated from 3 replicates with standard deviations expressed in error bars. Statistical analysis was performed by Paired-sample t-test using Microsoft Office Excel 2011 (Microsoft, Inc., U.S.A.). Means differ significantly from each other if $p < .05$, very significantly if $p < .01$.

3. Results and discussion

3.1. Water sorption analysis

In Table 2 the experimental water contents for freeze-dried emulsions (systems 1, 2, 3) over the whole range of water activities at 25 ± 2 °C after 360 h of storage are shown.

The sorption kinetics profiles for system 1 (Fig.1 a), 2 (Fig.1 b) and 3 (Fig.1 c) at different relative humidity demonstrate the time required for the system equilibration. At whole range of water activities, carbohydrate-protein system showed slightly higher amount of sorbed

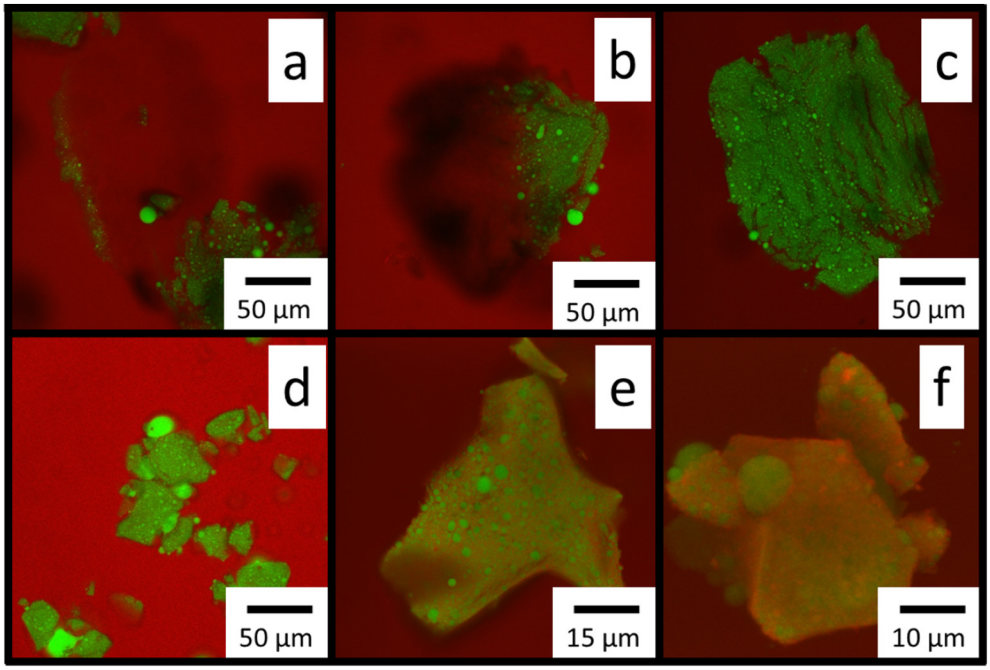

Fig. 5. Confocal scanning laser micrographs of showing internal microstructures of anhydrous system 2 (a, b, c) and system 3 (d, e, f). Figures are fluorescently labeled with Fast green/Nile red to show fat (green) and protein (red).

water followed by carbohydrate-protein-oil systems. The amount of sorbed water slightly decreased with increasing oil content, due to hydrophobic interactions between proteins and oils at the interface (Zhou & Roos, 2012).

Delayed trehalose crystallization was found at 0.76 a_w and above for all systems. The longer crystallization time compare to pure trehalose systems can be explained by complex interference and possible interactions between carbohydrates and protein, e.g. by hydrogen bonds between carbohydrates and proteins (Zhou & Roos, 2012). Also, oil in carbohydrate-protein-oil systems (system 2, 3) may cover particles by free fat layer that result in significant change of water sorption profile (Vignolles et al., 2007). The dispersed oil phases with protein interfaces disturbed the continuous hydrophilic carbohydrate-protein phase and slowed the movement of carbohydrate molecules to form crystals (Zhou & Roos, 2012).

The GAB model was fitted to the water sorption data for all systems. System 1 at the low experimental a_w range showed sigmoid sorption isotherm and highest water sorption, followed closely by system 2 and then system 3 (Fig. 2). The slight decrease of sorbed water amount in the system may be explained by hydrophobic interactions between protein and oil phases, which decreased the amount of protein in carbohydrate-protein fractions and their hydrogen bonding with water (Zhou & Roos, 2012).

3.2. Glass transition temperature

The glass transition temperature for anhydrous and humidified systems 1, 2 and 3 were read from second heating DSC thermographs. The T_g of all systems are shown in the Table 3.

The T_g values of anhydrous of humidified trehalose-WPI-SO systems were slightly higher than that of pure trehalose due to high protecting effect of trehalose on protein structures and possible proteins effect of anhydrous systems by hydrogen bonding to carbohydrate molecules (Lopez-Diez and Bone, 2004; Maidannyk & Roos, 2016; Zhou & Roos, 2012). System 1, 2 and 3 showed similar values of T_g. Slightly increased T_g values are in agreement with water sorption data. This finding supports that systems were plasticized by water resulting in the decrease of the T_g regardless of the presence of protein and oil (Levine & Slade, 1986; Roos & Karel, 1991; Silalai & Roos, 2011). Fig. 3a showed that glass transition occurred only in the nonfat solids components and the T_g values closely followed the carbohydrate component of system at whole a_w range (Maidannyk & Roos, 2016; Zhou & Roos, 2012).

The Gordon-Taylor equation was successfully fitted to experimental data of freeze-dried trehalose-WPI-SO systems (Fig. 3b). Experimental T_{g1} (Table 2) for anhydrous systems and $T_{g2} = -135$ °C (Angell, 2002) for water were used in calculations. For systems 1, 2 and 3 constants k were 7.2 ± 1.5; 7.4 ± 0.9 and 7.8 ± 1.3 respectively.

3.3. Dielectric and dynamic-mechanical properties

Structural α-relaxations usually occur in amorphous systems at temperatures close to the calorimetric glass transition temperature (Champion, Le Meste, & Simatos, 2000; Roudaut, Simatos, Champion, Contreras-Lopez, & Le Meste, 2004). For freeze-dried anhydrous and humidified systems (1, 2, 3), α-relaxation temperatures (T_α) were obtained from the peak temperature of dielectric loss (ε") and dynamic tan δ (tan δ = E"/E', where E" – loss modulus (mechanical energy dissipation), E' – storage modulus (mechanical energy storage)) of dielectric and dynamic mechanical analyses. Both DMA and DEA spectra are frequency-dependent, which allows obtaining the relaxation time – temperature dependence for amorphous systems (Eq. (3)) (Fan & Roos, 2016, 2017; Maidannyk & Roos, 2016, 2017, 2018; Potes et al., 2012; Silalai & Roos, 2011).

Peak of α-relaxation occurred at~ 20–30 °C above the onset T_g for the DMA measurements and up to~ 60–70 °C above the onset T_g for the DEA measurements. Systems with higher amount of SO showed significantly broadened and less intensive DMA and DEA peaks compared to the system without SO. For anhydrous samples, at all frequencies, T_α slightly decreased with increasing lipid content in the system, which could be caused by significant difference on powders surface composition (lubricant effect) which is in agreement with microscopies observations (Table 4). Trehalose acted as filler in the dry matrix which surround SO droplets. Also, free fat and fat droplets had the lower values of diffusion coefficients than trehalose and WPI hence they remained at the surface (Vignolles, Jeantet, Lopez, & Schuck, 2007). However, for humidified systems, we observed the opposite effect,

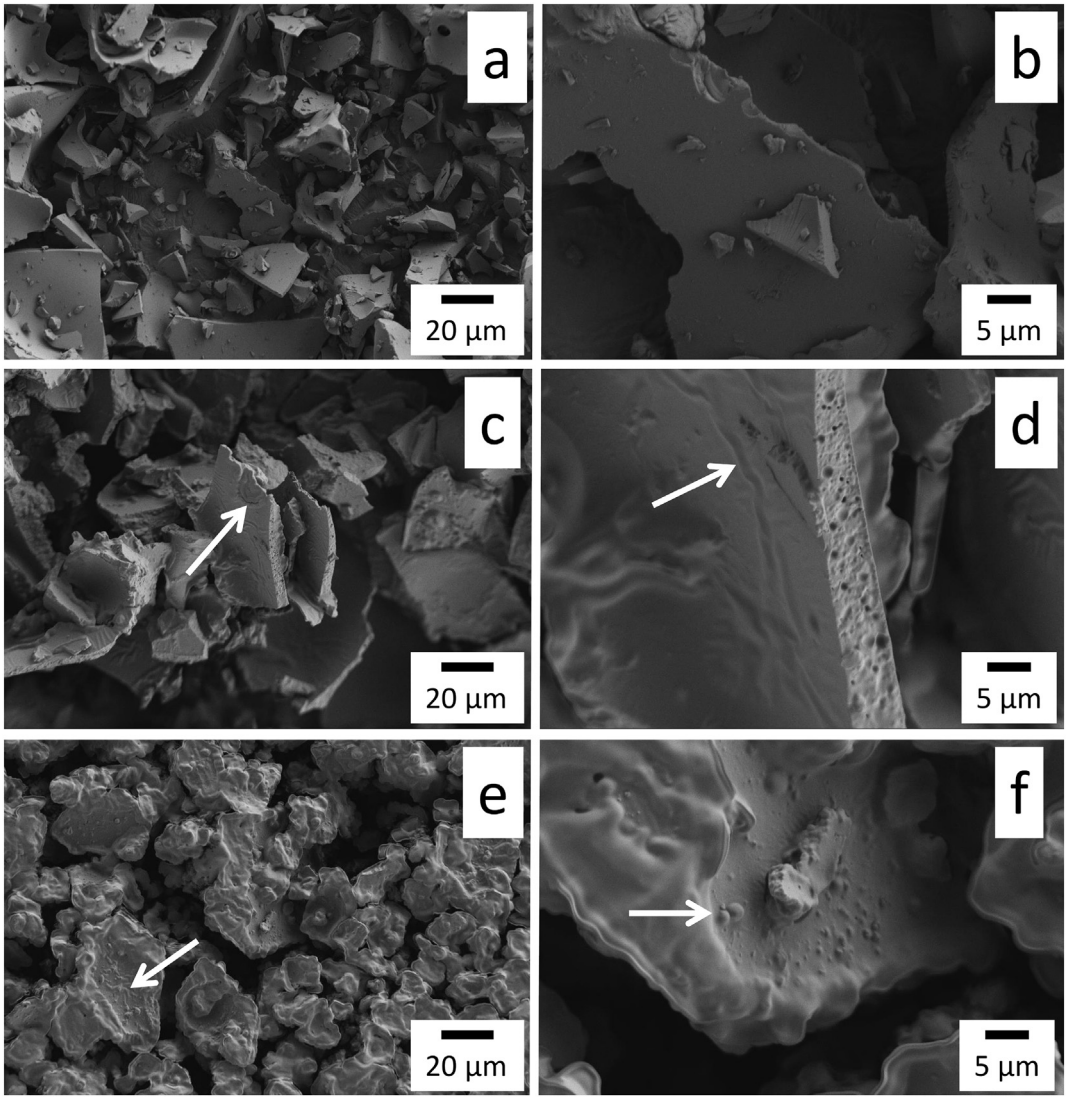

Fig. 6. Scanning electron micrographs of anhydrous system 1 (a, b), system 2 (c, d) and system 3 (e, f). Images shows powder particle surface morphology (a, c, e) and interior features of fractured particles (b, d, f). Arrows indicate fat globules and fat droplets.

Table 5
Calculated WLF constants C_1 and C_2 for amorphous systems 1, 2 and 3 stored at various relative humidities (RH).

System	System 1		System 2		System 3	
RH, %	$-C_1$, s	$-C_2$, °C	$-C_1$, s	$-C_2$, °C	$-C_1$, s	$-C_2$, °C
0	2.03 ± 0.17	61.9 ± 3.1	2.22 ± 0.29	54.2 ± 4.1	5.01 ± 0.65	67.4 ± 4.1
11	2.14 ± 0.33	50.9 ± 2.5	2.53 ± 0.32	47.1 ± 3.5	1.86 ± 0.47	39.7 ± 3.3
23	5.99 ± 0.22	66.8 ± 3.4	5.46 ± 0.42	53.2 ± 4.2	6.31 ± 0.46	54.5 ± 4.2
33	4.34 ± 0.18	51.7 ± 2.2	3.39 ± 0.29	38.2 ± 2.7	1.17 ± 0.21	22.4 ± 1.4
44	1.65 ± 0.24	30.7 ± 1.5	1.46 ± 0.17	25.1 ± 1.3	0.76 ± 0.15	20.7 ± 1.3

which is probably caused by the plasticizing effect in amorphous systems. T_α in all systems was found to decrease with increasing water content. All of these changes in systems can be explained by the free-volume theory, which shows that increasing free volume and molecular mobility significantly affected the T_g and T_α of amorphous sugar in a complex system (Meinders & van Vliet, 2009; Royall et al., 2005; Slade et al., 1991).

3.4. Microscopy

3.4.1. Optical light microscopy (OLM)

OLM was carried out on anhydrous freeze-dried systems 1, 2 and 3. Significant differences in particles transparency and shapes were observed between systems (Fig. 4). The transparency decreased with increasing SO content in the system. The layer of fat drops was observed in system 2 and 3. Also, the addition of SO makes the edges of particles smoother. No evidence of trehalose crystals was found in anhydrous systems 1, 2 and 3 in polarized light.

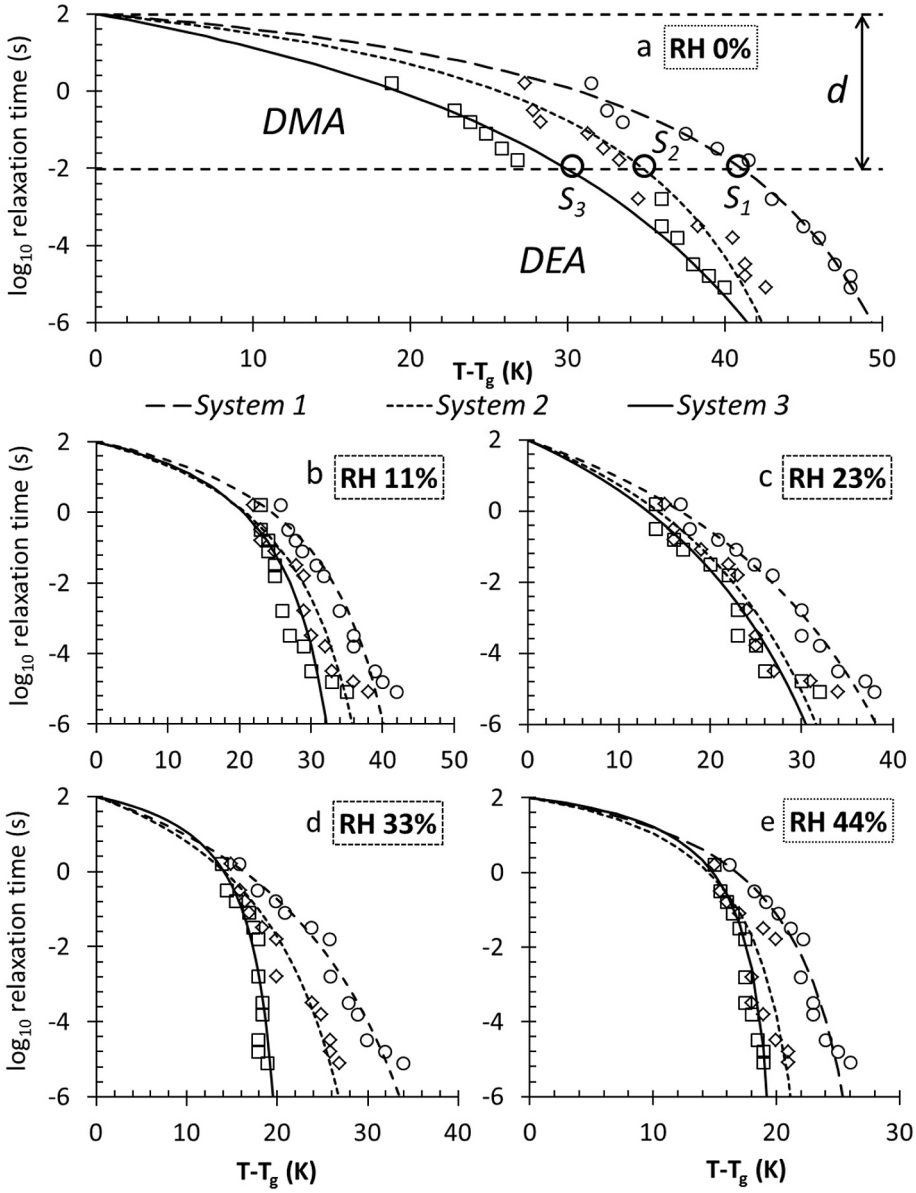

Fig. 7. Modified WLF curves (lines) and experimental data (symbols) for systems 1, 2 and 3 stored for 360 h at various relative humidity (0 (a), 11 (b), 23 (c), 33 (d) and 44% (e)) at 25 ± 1 °C.

Table 6
Strength S (at d = 4) for systems 1, 2 and 3 at different relative humidities (RH) and water contents.

Relative humidities/water content	System 1	System 2	System 3
RH 0%	41.0 ± 3.3	34.8 ± 2.7	29.9 ± 3.1
RH 11%	33.1 ± 2.8	30.1 ± 2.7	27.1 ± 2.8
RH 23%	26.7 ± 3.1	21.1 ± 3.1	21.1 ± 2.7
RH 33%	24.8 ± 4.1	20.6 ± 2.3	17.3 ± 3.5
RH 44%	21.7 ± 2.9	18.4 ± 2.5	17.3 ± 2.4

3.4.2. Confocal laser scanning microscopy

Confocal laser scanning microscopy results are shown in Fig. 5. Labeling with Fast Green/Nile Red dyes colored the fat and protein phases of system 2 (Fig. 5 a, b, c) and system 3 (Fig. 5 d, e, f) and showed air vacuoles as dark regions within the particle. Discrete spherical free fat green droplets (1–5 μm diameters) were observed in system 2 and 3 mostly on a particle surface which is in agreement with previous works (Maher et al., 2015; McKenna, 1997). System 3 shows

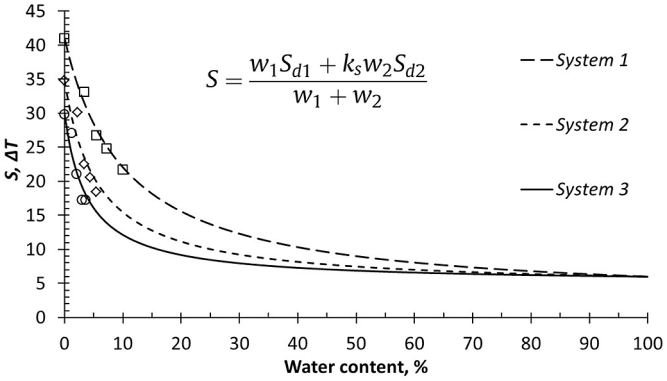

Fig. 8. Modeled by Eq. (9) (lines) and experimental (symbols) S systems 1, 2 and 3 at the different water contents.

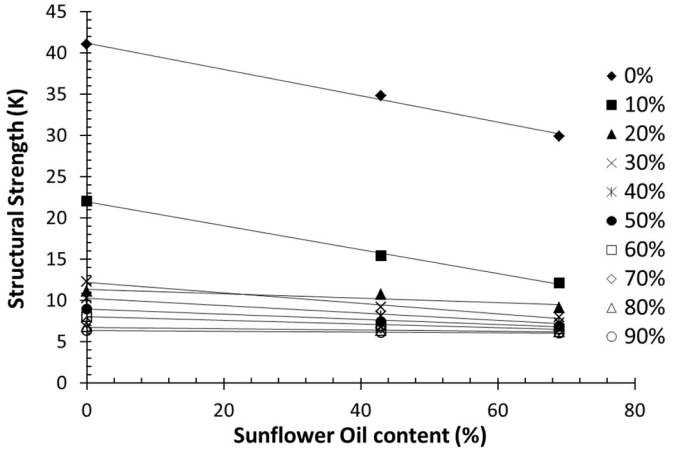

Fig. 9. The dependence of S from SO content (%) for systems 1, 2 and 3 at different water contents (The data predicted by Eq. (9)).

more free fat droplets than system 2 due to higher amount of fat in a system.

3.4.3. Scanning electron microscopy (SEM)

SEM is one of the most commonly used qualitative method to assess particle microstructure (Schmidt & Buchheimi, 1992; Kalab, 1979; Baechler, Clerc, Ulrich, & Benet, 2005). SEM pictures of fractured powders particles are presented in Fig. 6. System 1 (Fig. 6 a, b) showed very smooth surface while system 2 (Fig. 6 c, d) and system 3 (Fig. 6 e, f) have a characteristic fat globules. There was evidence of free fat on the surface of system 2, 3. System 2 and 3 shows an uneven distribution of oil droplets spread throughout the powder particles. The size of the oil droplets was from 150 to 1200 nm, similar to results of Maher et al. (2015). Higher magnifications showed the powder wall structure at nano-scale (Fig. 6 b, d, f). In system 2 and 3, spherical fat droplets of mostly 200 nm to 3 μm in diameter were seen embedded within the wall protein matrix.

3.5. WLF modeling and Strength

Williams-Landel-Ferry (WLF) equation is one of the traditional models of the temperature dependence on structural relaxation time (Williams et al., 1955). In the present study, "non-universal" constants C_1 and C_2 were calculated using Eq. (6) and assumption that the viscosity and relaxation time of supercooled liquid approached 10^{12} Pa s and 100 s respectively. Upon heating, values of viscosity and relaxation time decreased down to 10^5 Pa s and 10^{-14} s (Angell, 1991; Angell, 2002; Angell et al., 2000; Fan & Roos, 2016, 2017; Maidannyk et al., 2017; Maidannyk & Roos, 2016, 2017, 2018; Roos et al., 2015). Table 5 shows the WLF constants for anhydrous and humidified systems.

The introduction of WLF model to determine the flow characteristics or "strength" of amorphous materials (*S*) as described by Roos (Roos et al., 2015) enable direct comparison of structural relaxation times of different materials in the vicinity and above the glass transitions as T_g was used to standardize the temperature scale (Roos, 2013). Fig. 7 shows experimental data of DMA, DEA (symbols) and WLF curves (lines) with calculated C_1 and C_2 constants. During heating, a critical and large change in structural relaxation time occurred between 100 s and 0.01 s or between 2 and − 2 in logarithmic scale. The temperature difference, $T\text{-}T_g$, at which these changes happens, was defined as a "strength" parameter (S).

Strength parameter was calculated using Eq. (7). Table 6 presented data of Strength, which were calculated at $d = 4$.

Table 5 and Fig. 7 show that water, as a good plasticizer, significantly decreases strength of the system. Water is one of key factor for controlling properties, processes and storage stability for many food and pharmaceutical products (Liu et al., 2006). Previous studies (Fan & Roos, 2016; Fan & Roos, 2017; Maidannyk et al., 2017) developed an equation (Eq. (8)) for interpreting the relationship between water content and strength parameters. Such relationship was also applied for describing the influence on strength and water content of each system and achieved a very good fitting performance (Fig. 8). The *k* value was 10.6, 18.4 and 26.1 for the systems 1, 2 and 3 respectively.

System with the low amount of SO has more "strong" properties compare to the "weak" systems with high lipids content. Very big difference in strength values (~ 20 degree) was observed between anhydrous (RH 0%) systems 1 and 3 (Table 6, Fig. 7), that is in agreement with microscopy observation. SO presented on particle surface as free fat drops and fat globules may act as a lubricant and affect mechanical characteristics and electrical conductivity, that reduces overall strength of the system. It means that in systems with low amount of lipids, structural relaxation times achieved a critical level at lower temperatures than in trehalose-WPI systems. Similar effects were showed in our previous studies on carbohydrate-protein, miscible and semi-crystalline systems (Fan & Roos, 2016, 2017; Maidannyk et al., 2017; Maidannyk & Roos, 2016, 2017, 2018).

Systems with higher amount of sunflower oil show lower value of strength at any water content (Figs. 7, 8). *Structural strength* was decreasing *linearly* (with 0.9948, 0.9978, 0.8009, 0.9916, 0.9901, 0.9891, 0.9887, 0.9883, 0.9883, and 0.9874 R^2 for 0%; 10%; 20%; 30%; 40%; 50%; 60%; 70%; 80% and 90% of water respectively) with increasing SO concentration in the system (Fig. 9). Using *linear dependence*, experimental data (Table 5) and Eq. (8) allows prediction of S value at any lipids and water content in the system.

The present work confirms that strength approach is universal and can be applied for various food systems including systems containing fats. This model can find application in processing, quality control and storage stability of food products.

4. Conclusions

Strength analysis was applied for trehalose-WPI-SO systems with various contents of SO. Water sorption analysis allowed determining water content in freeze-dried amorphous systems at different water activities. The presence of lipids in the system prevents trehalose crystallization. For anhydrous system, the α-relaxation temperature was decreasing with increasing lipid content in the system. At the same time α-relaxation and glass transition temperature were decreasing with increasing water content in the systems. Microscopy observation showed that SO is presented as free fat and fat globules. Structural strength demonstrated linear dependence on the lipid concentration and significantly decreased with increasing of the water content. Knowing strength of pure anhydrous components allows predicting structural strength of mixture at any water contents. Present results can be useful in processing, characterization, product development as well as quality and stability control of various food products such as dairy powders and infant formulae.

Acknowledgments

This investigation was supported by the Food Institutional Research Measure (FIRM) project "Formulation and Design for Food Structure and Stability" funded by the Department of Agriculture, Food and Marine (11-F-001), coordinated by prof. Y.H. Roos, UCC, Ireland and by the Food Institutional Research Measure (FIRM) project "Developing the next generation of high protein spray dried dairy powders with enhanced hydration properties" (15-F-679) funded by the Department of Agriculture, Food and Marine, coordinated by Dr. Mark Auty, Teagasc Food Research Centre, Moorepark, Co. Cork, Ireland. Authors also thank Ms. Carolina Gomez in Teagasc Food Research Centre, Moorepark, Co. Cork, Ireland, for her kind assistance.

References

Angell, C. (2002). Liquid fragility and the glass transition in water and aqueous solutions. *Chemical Reviews, 102*(8), 2627–2650.

Angell, C. A. (1991). Thermodynamic aspects of the glass transition in liquids and plastic crystals. *Pure and Applied Chemistry, 63*(10), 1387–1392.

Angell, C. A., Ngai, K. L., McKenna, G. B., McMillan, P. F., & Martin, S. W. (2000). Relaxation in glassforming liquids and amorphous solids. *Journal of Applied Physics, 88*(6), 3113–3157.

Arvanitoyannis, I., Blanshard, J., Izzard, M., Lillford, P., & Ablett, S. (1993). Calorimetric study of the glass transition occurring in aqueous glucose: Fructose solutions. *Journal of the Science of Food and Agriculture, 63*(2), 177–188.

Auty, M. A., Twomey, M. Y. R. A., Guinee, T. P., & Mulvihill, D. M. (2001). Development and application of confocal scanning laser microscopy methods for studying the distribution of fat and protein in selected dairy products. *Journal of Dairy Research, 68*(3), 417–427.

Baechler, R., Clerc, M. F., Ulrich, S., & Benet, S. (2005). Physical changes in heat-treated whole milk powder. *Le Lait, 85*(4–5), 305–314.

Champion, D., Le Meste, M., & Simatos, D. (2000). Towards an improved understanding of glass transition and relaxations in foods: Molecular mobility in the glass transition range. *Trends in Food Science & Technology, 11*(2), 41–55.

Cornacchia, L., & Roos, Y. H. (2011). Lipid and water crystallization in protein-stabilised oil-in-water emulsions. *Food Hydrocolloids, 25*(7), 1726–1736.

Crowe, L. M., Crowe, J. H., Rudolph, A., Womersley, C., & Appel, L. (1985). Preservation of freeze-dried liposomes by trehalose. *Archives of Biochemistry and Biophysics, 242*(1), 240–247.

Debenedetti, P. G. (2003). Supercooled and glassy water. *Journal of Physics: Condensed Matter, 15*(45), R1669.

Ermolina, I., Polygalov, E., Bland, C., & Smith, G. (2007). Dielectric spectroscopy of low-loss sugar lyophiles: II. Relaxation mechanisms in freeze-dried lactose and lactose monohydrate. *Journal of Non-Crystalline Solids, 353*(47), 4485–4491.

Fan, F., & Roos, Y. H. (2016). Structural relaxations of amorphous lactose and lactose-whey protein mixtures. *Journal of Food Engineering, 173*, 106–115.

Fan, F., & Roos, Y. H. (2017). Structural strength and crystallization of amorphous lactose in food model solids at various water activities. *Innovative Food Science & Emerging Technologies, 40*, 27–34.

Green, J. L., & Angell, C. A. (1989). Phase relations and vitrification in saccharide-water solutions and the trehalose anomaly. *The Journal of Physical Chemistry, 93*(8), 2880–2882.

Halle, B. (2004). Protein hydration dynamics in solution: A critical survey. *Philosophical Transactions of the Royal Society B: Biological Sciences, 359*(1448), 1207–1224.

Hartel, R. (2001). Measurements of crystalline structure in foods. *Crystallization in Foods,* 34–90.

Kalab, M. (1979). Microstructure of dairy foods. 1. Milk products based on protein1. *Journal of Dairy Science, 62*(8), 1352–1364.

Kilmartin, P. A., Reid, D. S., & Samson, I. (2004). Dielectric properties of frozen maltodextrin solutions with added NaCl across the glass transition. *Journal of the Science of Food and Agriculture, 84*(11), 1277–1284.

Levine, H., & Slade, L. (1986). A polymer physico-chemical approach to the study of commercial starch hydrolysis products (SHPs). *Carbohydrate Polymers, 6*(3), 213–244.

Lim, A. S., Burdikova, Z., Sheehan, J. J., & Roos, Y. H. (2016). Carotenoid stability in high total solid spray dried emulsions with gum Arabic layered interface and trehalose–WPI composites as wall materials. *Innovative Food Science & Emerging Technologies, 34*, 310–319.

Liu, Y., Bhandari, B., & Zhou, W. (2006). Glass transition and enthalpy relaxation of amorphous food saccharides: A review. *Journal of Agricultural and Food Chemistry, 54*(16), 5701–5717.

López-Dıez, E., & Bone, S. (2004). The interaction of trypsin with trehalose: an investigation of protein preservation mechanisms. *Biochimica et Biophysica Acta (BBA)-General Subjects, 1673*(3), 139–148.

Maher, P. G., Auty, M. A. E., Roos, Y. H., Zychowski, L. M., & Fenelon, M. A. (2015). Microstructure and lactose crystallization properties in spray dried nanoemulsions. *Food Structure, 3*, 1–11.

Maidannyk, V., & Roos, Y. (2016). Modification of the WLF model for characterization of the relaxation time-temperature relationship in trehalose-whey protein isolate systems. *Journal of Food Engineering, 188*, 21–31.

Maidannyk, V. A., Nurhadi, B., & Roos, Y. H. (2017). Structural strength analysis of amorphous trehalose-maltodextrin systems. *Food Research International, 96*, 121–131.

Maidannyk, V. A., & Roos, Y. H. (2017). Water sorption, glass transition and "strength" of lactose–Whey protein systems. *Food Hydrocolloids, 70*, 76–87.

Maidannyk, V. A., & Roos, Y. H. (2018). Structural strength analysis of partially crystalline trehalose. *LWT-Food Science and Technology, 88*, 9–17.

McKenna, A. B. (1997). Examination of whole milk powder by confocal laser scanning microscopy. *Journal of Dairy Research, 64*(3), 423–432.

Meinders, M. B., & van Vliet, T. (2009). Modeling water sorption dynamics of cellular solid food systems using free volume theory. *Food Hydrocolloids, 23*(8), 2234–2242.

Noel, T. R., Parker, R., & Ring, S. G. (2000). Effect of molecular structure and water content on the dielectric relaxation behaviour of amorphous low molecular weight carbohydrates above and below their glass transition. *Carbohydrate Research, 329*(4), 839–845.

Özkan, N., Walisinghe, N., & Chen, X. D. (2002). Characterization of stickiness and cake formation in whole and skim milk powders. *Journal of Food Engineering, 55*(4), 293–303.

Potes, N., Kerry, J. P., & Roos, Y. H. (2012). Additivity of water sorption, alpha-relaxations and crystallization inhibition in lactose–maltodextrin systems. *Carbohydrate Polymers, 89*(4), 1050–1059.

Potes, N., Kerry, J. P., & Roos, Y. H. (2014). Protein modifications in high protein-oil and protein-oil-sugar systems at low water activity. *Food Biophysics, 9*(1), 49–60.

Prado, S. M., Buera, M. P., & Elizalde, B. E. (2006). Structural collapse prevents β-carotene loss in a supercooled polymeric matrix. *Journal of Agricultural and Food Chemistry, 54*(1), 79–85.

Roos, Y., & Karel, M. (1990). Differential scanning calorimetry study of phase transitions affecting the quality of dehydrated materials. *Biotechnology Progress, 6*(2), 159–163.

Roos, Y., & Karel, M. (1991). Phase transitions of mixtures of amorphous polysaccharides and sugars. *Biotechnology Progress, 7*(1), 49–53.

Roos, Y. H. (2008). *The glassy state, Food materials science.* Springer67–81.

Roos, Y. H. (2010). Glass transition temperature and its relevance in food processing. *Annual Review of Food Science and Technology, 1*, 469–496.

Roos, Y. H. (2013). Relaxations, glass transition and engineering properties of food solids. *Advances in food process engineering research and applications* (pp. 79–90). Springer.

Roos, Y. H., & Drusch, S. (2015). *Phase transitions in foods.* Academic Press.

Roos, Y. H., Fryer, P. J., Knorr, D., Schuchmann, H. P., Schroën, K., Schutyser, M. A., ... Windhab, E. J. (2015). Food engineering at multiple scales: Case studies, challenges and the future—A European perspective. *Food Engineering Reviews,* 1–25.

Roos, Y. H., & Potes, N. (2015). Quantification of protein hydration, glass transitions and structural relaxations of aqueous protein and carbohydrate-protein systems. *The Journal of Physical Chemistry B, 119*(23), 7077–7086.

Roudaut, G., Simatos, D., Champion, D., Contreras-Lopez, E., & Le Meste, M. (2004). Molecular mobility around the glass transition temperature: A mini review. *Innovative Food Science & Emerging Technologies, 5*(2), 127–134.

Royall, P. G., Huang, C.-y., Tang, S.-w. J., Duncan, J., Van-De-Velde, G., & Brown, M. B. (2005). The development of DMA for the detection of amorphous content in pharmaceutical powdered materials. *International Journal of Pharmaceutics, 301*(1), 181–191.

Schmidt, D. G., & Buchheimi, W. (1992). The application of electron microscopy in dairy research. *Journal of Microscopy, 167*(1), 105–121.

Silalai, N., & Roos, Y. H. (2011). Mechanical relaxation times as indicators of stickiness in skim milk–maltodextrin solids systems. *Journal of Food Engineering, 106*(4), 306–317.

Slade, L., Levine, H., & Reid, D. S. (1991). Beyond water activity: Recent advances based on an alternative approach to the assessment of food quality and safety. *Critical Reviews in Food Science & Nutrition, 30*(2–3), 115–360.

Soottitantawat, A., Yoshii, H., Furuta, T., Ohkawara, M., & Linko, P. (2003). Microencapsulation by spray drying: Influence of emulsion size on the retention of volatile compounds. *Journal of Food Science, 68*(7), 2256–2262.

Sperling, L. H. (2005). *Introduction to physical polymer science.* John Wiley & Sons.

Swenson, J., & Cerveny, S. (2015). Dynamics of deeply supercooled interfacial water. *Journal of Physics: Condensed Matter, 27*(3), 033102.

Vega, C., & Roos, Y. (2006). Invited review: Spray-dried dairy and dairy-like emulsions—Compositional considerations. *Journal of Dairy Science, 89*(2), 383–401.

Vignolles, M. L., Jeantet, R., Lopez, C., & Schuck, P. (2007). Free fat, surface fat and dairy powders: Interactions between process and product. *A review. Le Lait, 87*(3), 187–236.

Williams, M. L., Landel, R. F., & Ferry, J. D. (1955). The temperature dependence of relaxation mechanisms in amorphous polymers and other glass-forming liquids. *Journal of the American Chemical Society, 77*(14), 3701–3707.

Xie, G., & Timasheff, S. N. (1997). The thermodynamic mechanism of protein stabilization by trehalose. *Biophysical Chemistry, 64*(1), 25–43.

Zhou, Y., & Roos, Y. H. (2012). Stability and plasticizing and crystallization effects of vitamins in amorphous sugar systems. *Journal of Agricultural and Food Chemistry, 60*(4), 1075–1083.